

Research



Cite this article: Sigaeva T, Destrade M, Di Martino ES. 2019 Multi-sector approximation method for arteries: the residual stresses of circumferential rings with non-trivial openings.

J. R. Soc. Interface **16**: 20190023.

<http://dx.doi.org/10.1098/rsif.2019.0023>

Received: 14 January 2019

Accepted: 1 July 2019

Subject Category:

Life Sciences—Mathematics interface

Subject Areas:

biomechanics

Keywords:

residual stress, asymmetric openings, multi-sector approximation method, opening angle method

Author for correspondence:

Elena S. Di Martino

e-mail: edimarti@ucalgary.ca

Multi-sector approximation method for arteries: the residual stresses of circumferential rings with non-trivial openings

Taisiya Sigaeva¹, Michel Destrade^{3,4} and Elena S. Di Martino²

¹Schulich School of Engineering, and ²Civil Engineering/Centre for Bioengineering Research and Education, University of Calgary, Calgary, Canada

³School of Mathematics, Statistics and Applied Mathematics, National University of Ireland Galway, Galway, Republic of Ireland

⁴School of Mechanical and Materials Engineering, University College Dublin, Dublin, Republic of Ireland

TS, 0000-0001-6764-1089; MD, 0000-0002-6266-1221; ESDM, 0000-0002-8005-9445

The opening angle method is a popular choice in biomechanics to estimate residual stresses in arteries. Experimentally, it means that an artery is cut into rings; then the rings are cut axially or radially allowing them to open into sectors; finally, the corresponding opening angles are measured to give residual stress levels by solving an inverse problem. However, for many tissues, for example in pathological tissues, the ring does not open according to the theory into a neat single circular sector, but rather creates an asymmetric geometry, often with abruptly changing curvature(s). This phenomenon may be due to a number of reasons including variation in thickness, microstructure, mechanical properties, etc. As a result, these samples are often eliminated from studies relying on the opening angle method, which limits progress in understanding and evaluating residual stresses in real arteries. With this work, we propose an effective approach to deal with these non-trivial openings of rings. First, we digitize pictures of opened rings to split them into multiple, connected circular sectors. Then we measure the corresponding opening angles for each sub-sector. Subsequently, we can determine the residual stresses for individual sectors in a closed-ring configuration and, thus, approximate the circumferential residual bending effects.

1. Introduction

The determination of residual deformations is essential to analyse and understand the mechanical behaviour of soft biological tissues. Any incision inevitably leads to an opening; any material extraction similarly leads to a change in the geometry of both the extracted piece and the region from which it was extracted—all revealing the presence of residual stresses. The kinematics of these residual deformations, together with a proper material characterization, can be used to estimate the magnitude of the residual stresses, so that they can be accounted for when modelling complicated biological processes and mimicking *in vivo* loading states.

In particular in arteries, residual stresses are known to optimize the distribution of transmural stresses due to internal pressure in order to achieve better functionality [1,2]. The conventional experimental approach for detecting and evaluating residual stress in arteries is the *opening angle method*, where thin circumferential rings from an artery are cut axially/radially and open into single sectors, revealing that the rings were under stress; see [3,4] and figure 1*a*. The opening angles are then measured and used in analytical models to estimate the magnitude and distribution of the residual stresses [5]. Over the years, it has become apparent that this experiment is not capable of capturing the full residual stress distribution in all real arteries.

First, this experiment reveals residual circumferential bending deformations only, and axial residual deformations are neglected. However, an axial strip cut

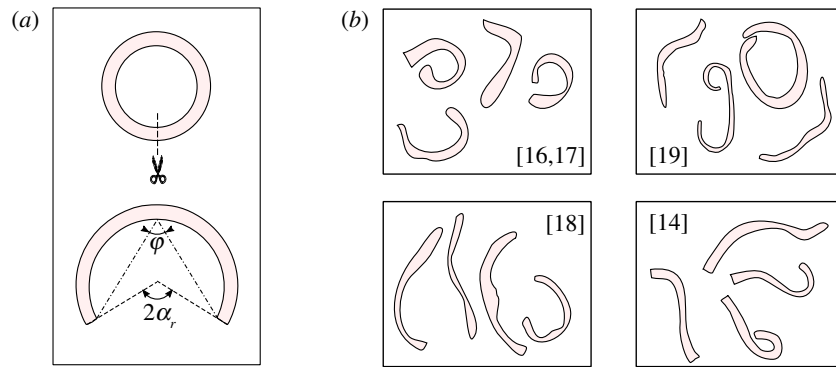


Figure 1. (a) Classical opening angle method, based on the assumption of an idealized circular sector opening. (b) Sketches of real openings reported and demonstrated in the literature (references in brackets). (Online version in colour.)

from the vessel (strip curling method [6]) can also exhibit a considerable bending deformation, or can undergo a considerable change in dimensions, or can experience both phenomena at the same time. This simple experiment reveals that axial residual deformations exist in arteries, that they play an important mechanical role [7], and that it is vital to account for them as they have a significant effect on the overall residual stress state. However, bending an axial strip significantly complicates the calculation of residual stresses in terms of analytical modelling, and many works prefer to neglect bending in either circumferential or axial strip [8], or both.

The next limitation of the conventional opening angle approach is that it ignores that arteries are multi-layered structures, and that each layer has different mechanical properties as well as different amounts and distributions of its main load-bearing components—elastin and collagen. As a result, even though stresses that were holding axial or circumferential strips in shape while being a part of the intact blood vessel are released, the stresses to hold the artery's incompatible layers together, or interface stresses, remain. Indeed, it has been shown that the three individual aortic layers, intima, media and adventitia, undergo drastically different residual deformations upon separation [9,10], requiring involved analytical models to calculate them [8]. These effects are demonstrated for both residual circumferential and axial bending deformations by means of the opening angle and strip curling methods, respectively.

Notwithstanding these limitations, the classical opening angle method introduced in the 1980s remains the most popular owing to its simplicity.

An estimation of the residual stresses based on the experimental observations of residual deformations can be done numerically with finite-element simulations and analytically using the methodology of large deformations universal to all nonlinear incompressible isotropic materials [11]. The models used to estimate the residual stress vary from the simplest homogeneous, isotropic ones to more advanced inhomogeneous, anisotropic ones that account for each layer's mechanics, microstructure and both circumferential and axial residual deformations [2]. Our focus in this work is the analytical approach.

In spite of decades of intense work dedicated to the study of residual stresses in soft tissues, their underlying mechanisms and their functions are still not fully understood [12]. It is accepted that they are strongly connected to growth and remodelling, which may actually trigger them. It is also established that external factors such as hypertension or

hypertrophy [13] can affect them. Residual stresses change with age [14]; they are different in different arteries and even along the same aorta. Clearly, any pathological changes affecting arteries will affect residual stresses too. Some researchers have even hypothesized that an incorrect functioning of residual stresses might cause pathology. In the aorta, for example, if the mechanism responsible for homeostatic deposition and degradation of collagen and elastin is not functioning properly, then an aneurysm is formed. Aneurysms may look like a localized ballooning of the aorta or may be more diffuse, but they are always associated with regional variations of properties along the circumference [15] and localized weakening. These local weak spots may be responsible for prospective dilatation or rupture of an aneurysm, which most often causes immediate death of the patient. This is one of the reasons why it is so important to be able to estimate accurately residual stresses in aneurysms.

Even though there has been considerable research into the improvement of analytical models estimating residual stresses and into the overall understanding of their role, there still remains one aspect related to the classical opening angle method that has not been properly addressed. Many experiments show that in some tissues, more commonly in the pathological ones, some rings do not open according to the theory, into a neat single circular sector, but instead create an asymmetric geometry, often with abruptly changing curvature(s).

Figure 1b shows sketches of the openings collected from several works: in the papers by Fung and collaborators [16,17] and Sokolis [18], we find notably asymmetric openings for porcine aortic rings from certain regions along the aorta; similarly in the papers by Okamoto *et al.* [19] and Sokolis *et al.* [14] for human aneurysms. In [19], rings which did not remain on edge after the cut and rings in which more than half the length fell over were excluded from the analysis. This happened because of either asymmetry or the need for physical support for the ring to remain in-plane when opened, or both. When a portion of the ring, but less than half, had fallen over, the opening angle was calculated using a special technique. Specifically, out of 55 patients and 55 corresponding rings, the opening angles could not be measured in 21 cases [19]. In [14], 16% of the total number of aortic rings were disregarded. These proportions may explain why there are so few studies of residual stresses in aneurysms, and also raise the question of how many samples were disregarded in other, non-aneurysmal, studies.

In this paper, we propose a simple, innovative and practical method to estimate residual stresses in asymmetric

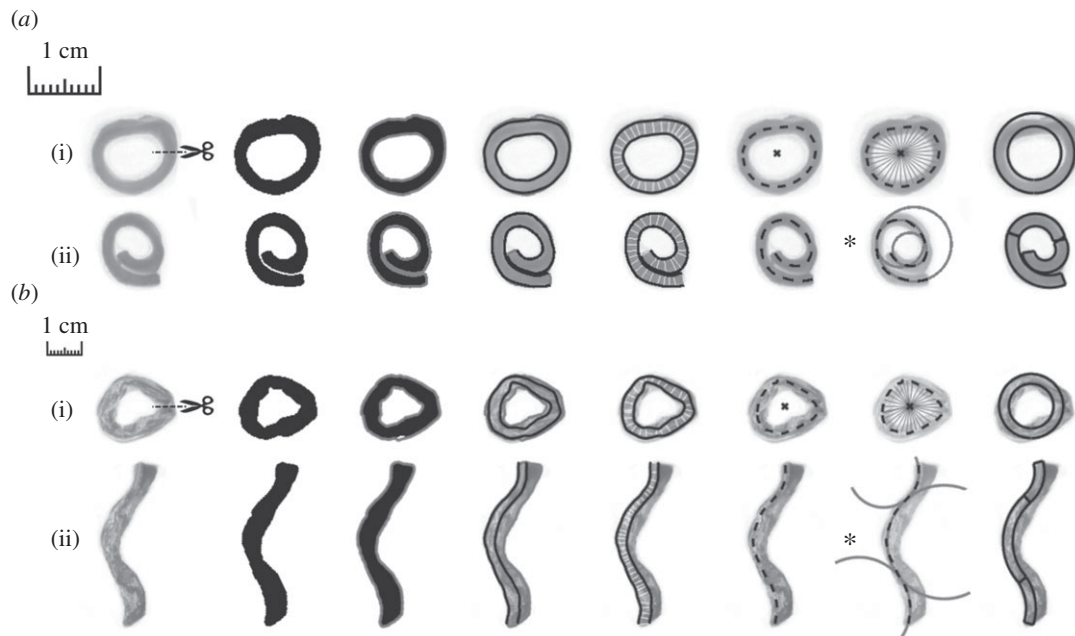


Figure 2. Digital image analysis steps for two samples: (a) pig AA and (b) human AAA. (i) Closed and (ii) opened configurations. Symbols (*) indicate the images which best illustrate the changes in curvature.

openings: we digitize asymmetric opened rings, split them into multiple sectors and measure the opening angle of each sub-sector (§2.1). Then, to determine residual stresses, we formulate the following inverse analytical approximation problem. Multiple undeformed sectors deform into multiple sectors with the same curvature, and with the only mathematical connection that deformed sectors should form a full ring (§2.2). With this approach, we can determine the non-homogeneous distribution of residual stresses for individual sectors in a closed-ring configuration (§3). These stresses will describe the residual circumferential bending stress states everywhere but at the edges between adjacent sectors, where we assume a complex, rapidly varying residual stress state. One can then either interpret the non-homogeneous residual stress distribution or simply look at its average. Analytically, this approach is not much more complicated than the classical opening angle model (see recent treatments in [20,21]).

2. Methods

2.1. Experiments and digital image analysis

Here, as a case study, we analyse the asymmetric openings of two aortic rings taken from two different aortas on separate occasions.

The first ring comes from a healthy porcine aorta (Landrace cross domestic pig, 32 kg, castrated male, approx. four months old), particularly its upper abdominal part, denoted as ‘pig AA’ (abdominal aorta). The second ring comes from a human abdominal aortic aneurysm (5.7 cm max. aneurysm in a 55-year-old male patient), denoted ‘human AAA’ (abdominal aortic aneurysm). Samples were collected at the Center for Bioengineering Research and Education, Schulich School of Engineering, University of Calgary, Calgary, Canada, following protocols approved by the ethics board. They were stored at -4°C and tested within a few hours from extraction. Both rings sliced from aortas were about 4 mm in height and cleared from connective tissues using surgical scissors. Then they were fully immersed in room temperature phosphate-buffered saline solution (PBS, $\text{pH}=7.4$) for 10 min and allowed to equilibrate before ‘closed configuration’ imaging. A single cut along the

anterior part of the aorta was performed using surgical scissors and the opening rings were subsequently left to rest for 10 min before the final ‘opened configuration’ image capture.

The digital image analysis of both closed and opened configurations was conducted using built-in and adapted functions of Matlab (version R2018a). We treated differently the closed and opened configurations. Closed configurations, although not perfectly circular, were considered circular. Here the main objective was to determine the mean aortic ring thickness and radius from the images. These quantities fully describe the geometry of the deformed, load-free ring. First, the image of the ring was binarized; as the human AAA sample had quite a bit of colour variation along the thickness, different thresholds were used for human AAA and pig AA samples. Next, a Sobel-based algorithm was used to detect the edges of the rings. As pointed out by Holzapfel *et al.* [9], these edges are just approximations of real boundaries, which are impossible to determine exactly, and they have to be manually adjusted for an optimal fit. Here the edges were represented as natural cubic spline curves with 30 knots, and these knots were manually dragged to reach a good correspondence with the real ring boundaries. This manual adjustment was not necessary for the pig AA sample but proved essential for the human AAA sample, as its boundaries were not clear. Next, the shortest distances between spline-approximated inner and outer edges were found and averaged to determine the mean thickness of the rings. Then the centroid of the binarized shape was found. Finally, the mid-line between the inner and outer spline edges was determined and the distance from its knots to the centroid was averaged to estimate the mean radius, as depicted in figure 2.

For the opened configurations, the initial steps were the same as for the closed configuration, but here the main goal was to determine the smallest number of individual arcs that would fit the mid-line between inner and outer spline edges. To do this, the Hough circle transform was used to fit the mid-line [22]; the arcs of the circles intersecting at points of abrupt curvature changes were then selected to represent the mid-line (figure 2). Their radii and slanted angles were determined (angles formed by rays passing through fitted circle intersections and sample ends). It was possible to represent both human AAA and pig AA opened rings with just three sectors. We note that for the human AAA there is a smooth transition between arcs and sectors, in contrast to the transitions in the pig AA sample.

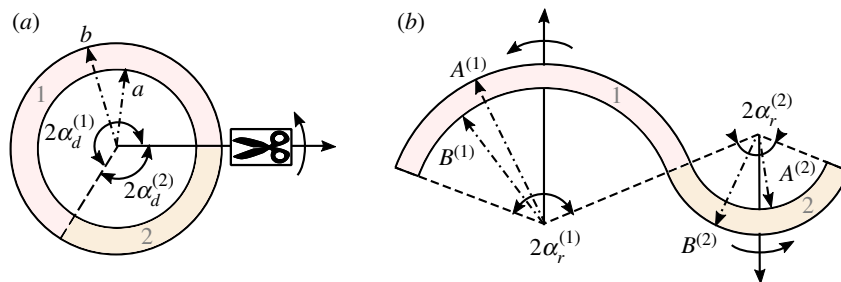


Figure 3. Closed, residually stressed, deformed (a) and open, stress-free, undeformed (b) configurations. (Online version in colour.)

It should be noted that the determination of the average thickness of the individual sectors in the opened configuration was challenging, as is often the case when dealing with irregular and heterogeneous strips of tissue after pathological remodelling.

2.2. Closing of N sectors into an intact tube

Assume that we have N joint sectors from different circular-cylindrical tubes. With the following plane-strain bending deformations:

$$r = r^{(i)}(R), \quad \theta = \kappa^{(i)}\Theta, \quad z = \lambda_z^{(i)}Z, \quad (i = 1 \dots N), \quad (2.1)$$

they form a closed intact tube occupying the region

$$a \leq r \leq b, \quad 0 \leq \theta \leq 2\pi, \quad 0 \leq z \leq \ell. \quad (2.2)$$

Here (R, θ, Z) are the coordinates of the cylindrical system aligned with the unit vectors $(\mathbf{E}_R, \mathbf{E}_\theta, \mathbf{E}_Z)$ in the undeformed (open, stress free) configuration, and (r, θ, z) and $(\mathbf{e}_r, \mathbf{e}_\theta, \mathbf{e}_z)$ are their counterparts in the deformed (closed, residually stressed) configuration. Also, $\lambda_z^{(i)}$ is the axial stretch of the i th sector and $\kappa^{(i)}$ reflects the change in the central angles between the i th sector's undeformed and deformed configurations.

Each sector $i = 1 \dots N$ occupies its own portion of the tube defined as

$$-\alpha_d^{(i)} \leq \theta^{(i)} \leq \alpha_d^{(i)}, \quad \text{with } \theta^{(i)} = \theta - \alpha_d^{(i)} - \sum_{k=1}^{i-1} 2\alpha_d^{(k)}. \quad (2.3)$$

Here $\theta^{(i)}$ is the conveniently chosen subsidiary circumferential coordinate used to locate the position of the deformed sectors $i = 1 \dots N$. When $i = 1$, the sector is located at $\theta \in [0, 2\alpha_d^{(1)}]$; when $i = 2$, it is located at $\theta \in [2\alpha_d^{(1)}; 2\alpha_d^{(1)} + 2\alpha_d^{(2)}]$, etc. Clearly, the following condition must hold:

$$\sum_{i=1}^N \alpha_d^{(i)} = \pi, \quad (2.4)$$

so that all sectors are joined into a full circle (condition of kinematical compatibility between sectors).

Undeformed sectors $i = 1 \dots N$ need to be either bent, unbent or everted to form a closed intact tube. Solution (2.1), as the most general plane-strain bending solution, is capable of capturing all these deformations via a single parameter $\kappa^{(i)}$. If we denote the central angle of the i th undeformed sector as $2\alpha_r^{(i)}$, then $\kappa^{(i)}$ can be expressed as

$$\kappa^{(i)} = \frac{\alpha_d^{(i)}}{\alpha_r^{(i)}} \in \left[-\frac{\pi}{\alpha_r^{(i)'}} , \frac{\pi}{\alpha_r^{(i)'}} \right] \setminus \{0\}, \quad (2.5)$$

$$\left(\alpha_r^{(i)} \in (0, \pi], \alpha_d^{(i)} \in [-\pi, \pi] \setminus \{0\} \right).$$

Therefore, $\kappa^{(i)} > 1$ corresponds to regular plane-strain bending, $\kappa^{(i)} \in (0, 1]$ corresponds to unbending, $\kappa^{(i)} < 0$ corresponds to unbending beyond the configuration of a rectangular block, i.e. eversion.

Assume that there are N_1 sectors that were bent and unbent from their undeformed states and N_2 sectors that were everted, so that $N_1 + N_2 = N$. We will use the sets $\mathbf{N}_1 = \{i \in [1, N] : \kappa^{(i)} >$

$0\}$ and $\mathbf{N}_2 = \{i \in [1, N] : \kappa^{(i)} < 0\}$ to differentiate between these sectors. If we define the undeformed radii as $R(a) \equiv A^{(i)}$ and $R(b) \equiv B^{(i)}$, then the sectors from sets \mathbf{N}_1 and \mathbf{N}_2 will occupy the following regions:

$$A^{(i)} \leq R \leq B^{(i)}, \quad -\alpha_r^{(i)} \leq \Theta \leq \alpha_r^{(i)}, \quad 0 \leq Z \leq L^{(i)}, \quad \text{when } i \in \mathbf{N}_1 \quad (2.6)$$

$$\text{and } B^{(i)} \leq R \leq A^{(i)}, \quad \alpha_r^{(i)} \leq \Theta \leq -\alpha_r^{(i)}, \quad 0 \leq Z \leq L^{(i)}, \quad (2.7)$$

when $i \in \mathbf{N}_2$.

The corresponding deformation gradients $\mathbf{F}^{(i)}$ are

$$\mathbf{F}^{(i)} = \frac{dr^{(i)}}{dR}(R)\mathbf{e}_r \otimes \mathbf{E}_r + \frac{\kappa^{(i)}r}{R}\mathbf{e}_\theta \otimes \mathbf{E}_\theta + \lambda_z^{(i)}\mathbf{e}_z \otimes \mathbf{E}_z, \quad (2.8)$$

$$\lambda_z^{(i)} = \frac{l}{L^{(i)}} \quad (i = 1 \dots N).$$

Taking the sectors to be incompressible, $\det \mathbf{F}^{(i)} = 1$ must hold at all times, from which we deduce that

$$r^{(i)} = \sqrt{\frac{R^2 - (A^{(i)})^2}{\kappa^{(i)}\lambda_z^{(i)}} + a^2}, \quad b = \sqrt{\frac{(B^{(i)})^2 - (A^{(i)})^2}{\kappa^{(i)}\lambda_z^{(i)}} + a^2} \quad (2.9)$$

$(i = 1 \dots N),$

so that the principal stretches can be expressed as

$$\lambda_r^{(i)} = \frac{R}{|\kappa^{(i)}|\lambda_z^{(i)}r}, \quad \lambda_\theta^{(i)} = \frac{|\kappa^{(i)}|r}{R} \quad \text{and} \quad \lambda_z^{(i)}.$$

For sectors made of incompressible, isotropic and hyperelastic material with strain energy density $W = W(I_1, I_2)$, the constitutive law for the Cauchy stress tensor $\boldsymbol{\sigma}$ is

$$\boldsymbol{\sigma} = -p\mathbf{I} + 2W_1\mathbf{B} - 2W_2\mathbf{B}^{-1}, \quad (2.10)$$

where p is the Lagrange multiplier introduced to ensure incompressibility, \mathbf{I} is the identity tensor, $\mathbf{B} = \mathbf{F}\mathbf{F}^T$ is the left Cauchy–Green deformation tensor and $W_i = \partial W / \partial I_i$ ($i = 1, 2$) with invariants $I_1 = \text{tr} \mathbf{B}$ and $I_2 = \text{tr} \mathbf{B}^{-1}$. It follows that, for the deformations (2.1), the Cauchy stress tensors $\boldsymbol{\sigma}^{(i)}$ for sectors $i = 1 \dots N$ have the following structure:

$$\boldsymbol{\sigma}^{(i)} = \sigma_{rr}^{(i)}\mathbf{e}_r \otimes \mathbf{e}_r + \sigma_{\theta\theta}^{(i)}\mathbf{e}_\theta \otimes \mathbf{e}_\theta + \sigma_{zz}^{(i)}\mathbf{e}_z \otimes \mathbf{e}_z. \quad (2.11)$$

As the components of the deformation gradients (2.8) do not depend on θ and z , we readily deduce from the equilibrium equations that for each sector $p^{(i)} = p^{(i)}(r)$ only, and that

$$\frac{d\sigma_{rr}^{(i)}}{dr} + \frac{\sigma_{rr}^{(i)} - \sigma_{\theta\theta}^{(i)}}{r} = 0, \quad (i = 1 \dots N), \quad (2.12)$$

are the only non-trivial equations of equilibrium. They are to be solved subject to the following boundary conditions of traction-free inner and outer faces of the deformed sectors:

$$\sigma_{rr}^{(i)}(a) = \sigma_{rr}^{(i)}(b) = 0, \quad (i = 1 \dots N). \quad (2.13)$$

Note that the normal forces on the deformed sub-sectors' end faces are all zero, and thus continuous in the closed ring.

Table 1. Results from the digital image analysis: in the undeformed configuration, $\alpha_r^{(i)}$ is the opening angle of the i th sub-sector and $C^{(i)}$ is its mid-line radius; in the deformed configuration, a and b are the inner and outer radii of the ring, respectively (figure 3).

configuration	pig AA sample		human AAA sample		
undeformed		$\alpha_r^{(i)}$	$C^{(i)}$, mm	$\alpha_r^{(i)}$	$C^{(i)}$, mm
	sector 1	103.18°	2.25	− 33.1°	10.4
	sector 2	74.59°	3.15	44.46°	16.8
	sector 3	63.59°	4.95	− 25.26°	15.2
deformed		a , mm	b , mm	a , mm	b , mm
		3.56	5.33	6.6	9.47

Where is this approach valid? From figure 2, we observe that the sectors in the opened configuration often exhibit regions where the curvature is approximately constant, and also transition regions where the curvature changes rapidly. Our analytical model is not expected to be valid in the vicinity of the transition regions, as it gives a point-wise discontinuity in the stress between the sectors when closed into the ring (the normal forces on each end face of the sectors are zero, and thus continuous), and a discontinuity in the moments. In reality, the stress and resulting moment states in these regions are too complicated to be captured by the present simplified model, which is geometrically oriented.

3. Numerical analysis

3.1. Solution procedure

All the necessary geometric parameters for both the human AAA and pig AA samples required for the analytical modelling are summarized in table 1.

We fully determined the deformed configurations of the samples, described by the inner and outer radii a and b . As for the undeformed configuration of each sample, it is described by three sectors with mid-lines radii $C^{(i)} = (A^{(i)} + B^{(i)})/2$ ($i = 1, 2, 3$) and the corresponding referential angles $\alpha_r^{(i)}$. The undeformed thicknesses $H^{(i)} = |B^{(i)} - A^{(i)}|$ ($i = 1, 2, 3$) of the sectors are deliberately left unfixed in the solution of the analytical problem. For the same reason, $C^{(i)}$ is reported instead of $A^{(i)}$ and $B^{(i)}$, as these quantities can be determined once $C^{(i)}$ and $H^{(i)}$ are known.

We note straight away that the undeformed sectors for the pig AA sample experience bending and unbending, while the sectors for the human AAA, in addition to regular bending, undergo eversion, which is reflected in the negative sign of $\alpha_r^{(1)}$ and $\alpha_r^{(3)}$.

The sectors can be modelled using any material model by prescribing the strain energy density function W . Ideally, this model should account for both mechanical and microstructural properties of cardiovascular tissues as well as anisotropy and nonlinearity. Here, for illustrative purposes and due to the absence of mechanical/microstructural data for our samples, we chose the simple isotropic neo-Hookean material, with strain energy density function

$$W^{(i)} = \frac{\mu^{(i)}}{2} (I_1^{(i)} - 3), \quad (3.1)$$

where $\mu^{(i)}$ is the shear modulus.

For each sample, there are seven equations to satisfy: the joining condition (2.4), the three equilibrium equations (2.12) and the three boundary conditions (2.13). Which seven unknowns should be selected to solve this problem?

Clearly, it is quite challenging to measure experimentally the deformed angles $\alpha_d^{(i)}$ ($i = 1, 2, 3$) formed by the sectors in the closed configuration; instead, we treat them as three variables to be determined from the analysis.

Next, it is clear that three sectors with different referential angles $\alpha_r^{(i)}$ and mid-line radii $C^{(i)}$ do not close into sectors with the same curvature and thickness $h = b - a$. Here we can take one of three routes. We can assume that sectors have different mechanical and microstructural properties, or that they have different axial deformations in closing $\lambda_z^{(i)}$, or that they have different undeformed thicknesses $H^{(i)}$ ($i = 1, 2, 3$).

Owing to the absence of mechanical data for the individual sectors, we have to assume that the material along the circumference of the aorta is homogeneous, i.e. $\mu^{(1)} = \mu^{(2)} = \mu^{(3)} = \mu$. Therefore, our choice of strain energy density functions (3.1) makes our solution independent of the shear modulus μ , which may thus be removed from the analysis by way of non-dimensionalization, i.e. by using $\sigma^{(i)}/\mu$ as the measure of stress (which we call $\sigma^{(i)}$ for convenience from now on). Accounting for the shear modulus of samples would result in a scaling of the residual stresses, but the qualitative results would remain the same.

Hence, in our numerical simulations we have to assume that the undeformed sectors opened asymmetrically either because of variations in wall thickness $H^{(i)}$ or because of differences in residual axial deformations $\lambda_z^{(i)}$ ($i = 1, 2, 3$). In the first scenario, we would have to assume that the $\lambda_z^{(i)}$ are the same for all sectors ($\lambda_z^{(1)} = \lambda_z^{(2)} = \lambda_z^{(3)} = \lambda_z$, say); in the second scenario, that the $H^{(i)}$ are the same for all three sectors ($H^{(1)} = H^{(2)} = H^{(3)} = H$, say). One may argue that, in general, the $\lambda_z^{(i)}$ are harder to measure than the $H^{(i)}$. However, thickness measurements can also be challenging for a given sample, especially for pathological tissues such as a human AAA sample.

3.2. Numerical results

Tables 2 and 3 display the results from the solution procedure described in the previous section.

When we assume that the ring opens asymmetrically owing to differences in the residual axial deformations $\lambda_z^{(i)}$ ($i = 1, 2, 3$), we find for the pig AA sample that the undeformed sectors have to be contracted axially ($\lambda_z^{(i)} < 1$) in order to close into the full ring (table 2). The common thickness of the undeformed sectors, $H = 1.71$ mm, is smaller than the thickness of the deformed ring, $h = b - a = 1.77$ mm. The undeformed sectors of the human AAA sample, in contrast, have to be pre-stretched axially ($\lambda_z^{(i)} > 1$) when closed, so that their initial thickness $H = 3.05$ mm is larger than the

Table 2. Results from the solution procedure when there is no variation in the wall thicknesses. Here $\alpha_d^{(i)}$ is the opening angle, $\lambda^{(i)}$ is the axial contraction found for the i th sub-sector, and $H = H^{(1)} = H^{(2)} = H^{(3)}$ is the common thickness (in millimetres).

	pig AA sample			human AAA sample		
	$\alpha_d^{(i)}$	H , mm	$\lambda_z^{(i)}$	$\alpha_d^{(i)}$	H , mm	$\lambda_z^{(i)}$
sector 1	52.97°	1.71	0.96	43.41°	3.05	1.05
sector 2	53.92°		0.95	88.82°		1.11
sector 3	73.11°		0.94	47.77°		1.06

Table 3. Results from the solution procedure when there is no variation in the residual axial deformations. Here $\alpha_d^{(i)}$ is the opening angle, $H^{(i)}$ is the thickness found for the i th sub-sector, and $\lambda = \lambda_z^{(1)} = \lambda_z^{(2)} = \lambda_z^{(3)}$ is the common axial pre-stretch.

	pig AA sample			human AAA sample		
	$\alpha_d^{(i)}$	$H^{(i)}$, mm	λ_z	$\alpha_d^{(i)}$	$H^{(i)}$, mm	λ_z
sector 1	53.21°	1.70	0.95	42.71°	3.10	1.08
sector 2	54.01°	1.71		89.98°	3.01	
sector 3	72.78°	1.72		47.31°	3.08	

thickness of the resulting ring $h = b - a = 2.87$ mm. Moreover, we notice that sector 2 requires more axial pre-stretch than sectors 1 and 3. This is not surprising when considering that sectors 1 and 3 went through significant eversion deformations; sector 2 was bent to a smaller degree; and all sectors had to have the same thickness when closed into the single ring (according to the assumption that a and b are fixed).

We find qualitatively similar results when we assume that the ring opens asymmetrically because of differences in the thickness $H^{(i)}$ ($i = 1, 2, 3$) along the circumference; see table 3. We see that, for the pig AA sample, the variation in thickness is not considerable, similarly to the minor variation between the axial pre-stretches in the previous case. For the human AAA sample, we see that sectors 1 and 3 undergo more significant changes in thickness to ensure compatibility with sector 2.

Note that we could have equally started with a ‘mixed’ case, where thickness and axial stretch of some sectors are assumed to be the same, so that the problem is solved for combinations of axial pre-stretches and thicknesses. Potentially, this strategy could be beneficial for the human AAA sample, where sectors 1 and 3 have similar deformations; so that the determined changes in height and thickness may be less substantial. Also, the thickness of the sectors in the ring configuration do not have to be the same, which can be accounted for in a subsequent version of the proposed model.

Note also that we do not discard the possibility of the microstructure and/or mechanics causing significant changes between the undeformed and deformed sectors’ thicknesses and heights; as stated earlier, this information can be easily included in the proposed model. This possibility is more relevant for the human AAA sample than for the pig AA sample as healthy pig tissues are fairly homogeneous, while tissues of abdominal aortic aneurysms are quite inhomogeneous and may have local weak zones.

As there is no substantial difference in results between the cases when asymmetric opening occurred due to variation in

wall thickness $H^{(i)}$ or due to different residual axial deformations $\lambda_z^{(i)}$ ($i = 1, 2, 3$), we depict the corresponding principal stretches and transmural residual stress states for all sectors of both samples for the first case only (i.e. when $H^{(1)} = H^{(2)} = H^{(3)} = H$) in figures 4 and 5. The grey arrows along the curved sides of the sub-sectors in the closed configuration indicate whether these sides are in tension or compression (figures 4a and 5a).

Sectors forming the opened configuration geometry of the pig AA sample experience different types of residual stress state when closed into the ring (figure 4a). The outer faces of sectors 1 and 2 are circumferentially and axially compressed, while their inner face is under tension (figure 4a–c). We also observe positive radial residual stress (figure 4c), as is typical for unbent structures. Sector 3, in contrast, does not appear as stressed as the other two sectors when closed (figure 4c). It also experiences bending and, as a result, has the opposite residual stress state when part of the closed ring (figure 4c). Also, its inner side is in compression, and its outer side is in tension (figure 4a–c).

For the human AAA sample, all three sectors experience positive radial residual stress throughout, tension on their outer face and compression on their inner face in the closed-ring configuration (figure 5). However, the sub-sectors that underwent eversion to close into the ring, i.e. sectors 1 and 3, experience much larger stresses than the sector in between them, sector 2, which was just bent (figure 4b).

3.3. Discussion

We now compare our treatment of pig AA and human AAA opened rings with the one that would be expected based on the classical opening angle method.

Okamoto *et al.* [19] and Solkolis [18] report difficulties in measuring opening angles for a large proportion of their samples. In these works, the opening angle is defined as the angle formed by two lines drawn from the tips of the inner

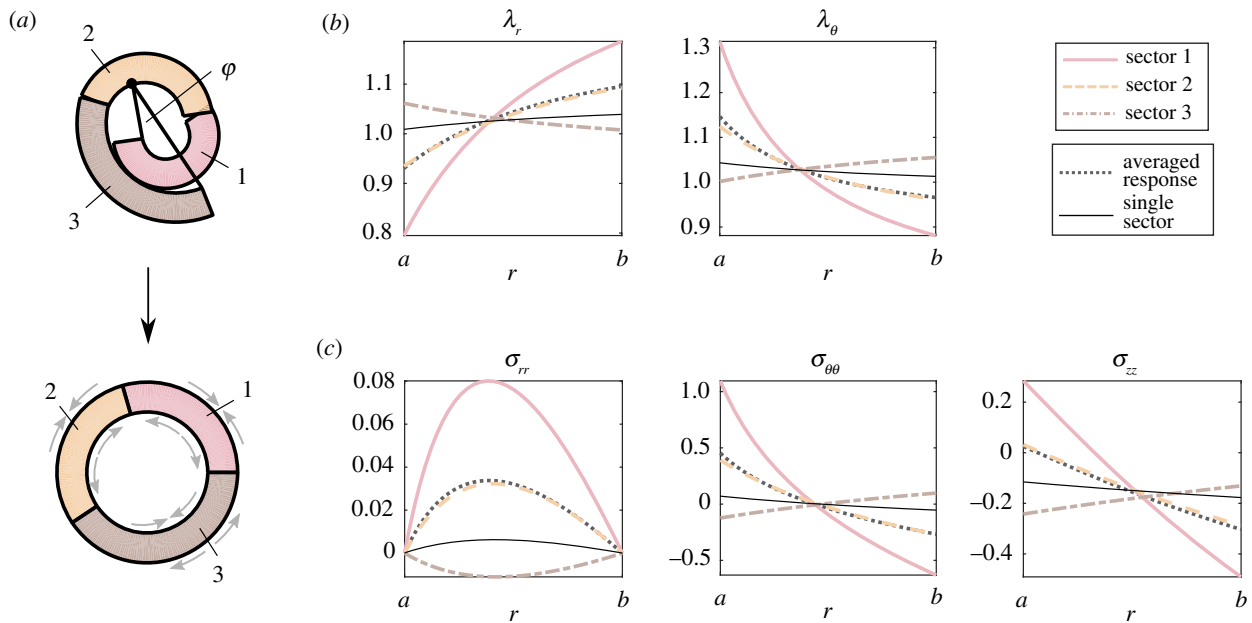


Figure 4. Pig AA sample: (a) kinematics, (b) principal stretches and (c) non-dimensionalized transmurals stress components for the case of three sub-sectors with the same thickness ($H^{(1)} = H^{(2)} = H^{(3)} = H$). (Online version in colour.)

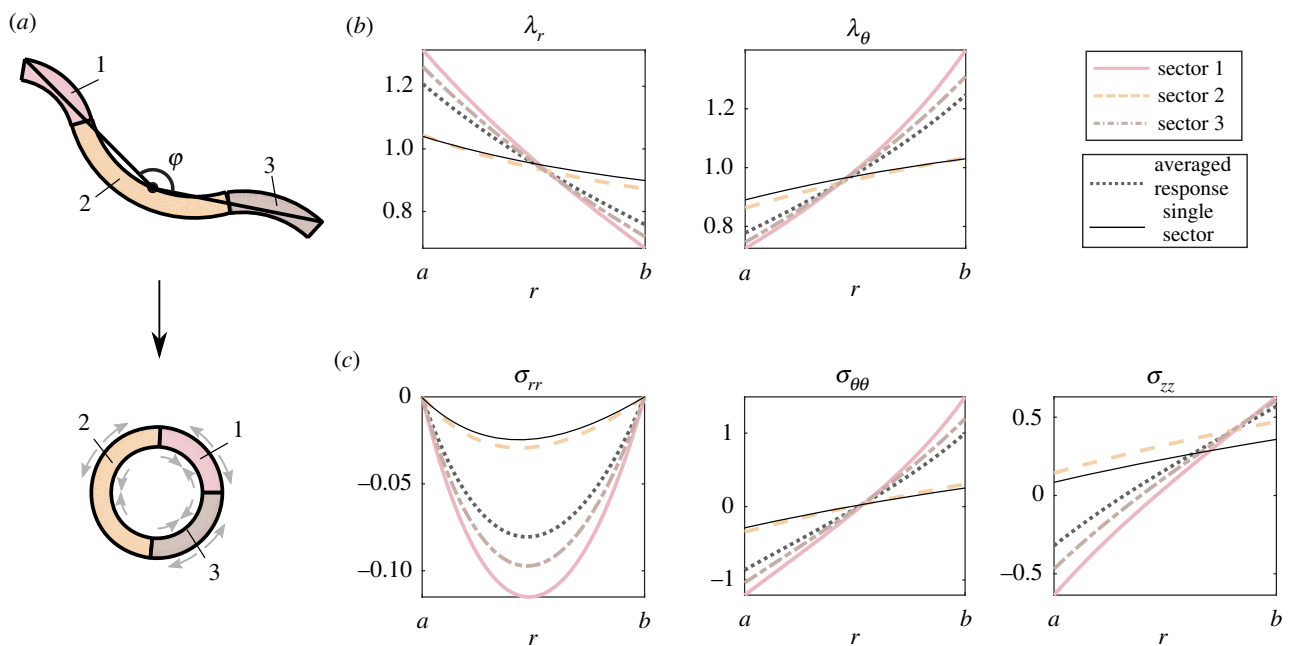


Figure 5. Human AAA sample: (a) kinematics, (b) principal stretches and (c) non-dimensionalized transmurals stress components for the case of three sub-sectors with the same thickness ($H^{(1)} = H^{(2)} = H^{(3)} = H$). (Online version in colour.)

circumference of the cut ring (intimal side) to its midpoint; see angle φ in figure 1a. The corresponding referential angle α_r is related to φ via the formula $\alpha_r = (2\pi - \varphi)/2$. We note that opened rings with abruptly changed curvature were excluded from these studies.

We measured the opening angles of our samples using this technique: we found that $\varphi = -26.38^\circ$ for the pig AA sample (figure 4a) and $\varphi = 146.21^\circ$ for the human AAA sample (figure 4b). The corresponding central angles for these openings are: $\alpha_r = 193.19^\circ$ and $\alpha_r = 106.9^\circ$, respectively; while $\alpha_d = 180^\circ$. The corresponding residual stress state can be easily determined using solution (2.1) for the case $N = 1$.

To properly compare residual stresses from the classical opening angle method with the residual stresses from our multi-sector

method, the following precautions need to be taken. First, the axial pre-stretch λ_z in the classical opening angle method should be in line with the results of the solution for the multiple sector approach: thus, we take $\lambda_z = 0.95$ for the pig AA sample; $\lambda_z = 1.08$ for the human AAA sample (based on the results of table 3). Second, as the multi-sector approach produces different residual stresses for each sector, we compute their average to provide a meaningful comparison with the single-sector opening angle method (the stress-based average). Figures 4c and 5c display both the averaged residual response from the multiple sector approach and the stresses resulting from the classical opening angle method, calculated for a single sector.

As can be seen in figure 4c, the single-sector opening angle method approach underestimates the residual stresses

in the pig AA ring. Indeed we expect that the opened ring has to experience significant circumferential tension when unfolding into a ring: here, however, the opening angle method predicts a $\sigma_{\theta\theta}$ very close to zero throughout the thickness of the arterial wall. The proposed multi-sector approach allows for a far more pronounced variation of $\sigma_{\theta\theta}$ (and, indeed, of σ_{rr} and σ_{zz}) in this sample.

Turning now to the human AAA sample, (figure 5c) we again observe that the calculated residual stresses based on the averaged response from the multi-sector approximation method are much higher than the stress yielded by the classical opening angle method. Moreover, because of abrupt changes in curvature, we conjecture that this sample most likely would have been eliminated if the spirit of [18,19] had been adhered to. Our approach clearly demonstrates that the sample can be used.

The final point to touch upon in this discussion is how to use and exploit the results coming from the multi-sector approach. One intuitive route to follow is to use the averaged response of the stress components across the thickness; see dotted lines in figures 4 and 5. It accounts for all opening angles in a single study, without having to eliminate any sample that does not follow the scenario of the single-sector opening angle method. With the averaged response, we can solve the inverse problem and report the values of α_r and λ_z . For our samples, we determined the following averaged values: $\bar{\alpha}_r = 252^\circ$ ($\bar{\varphi} = -144^\circ$ and $\bar{\lambda}_z = 0.95$ for the pig AA; $\bar{\alpha}_r = -23.72^\circ$ ($\bar{\varphi} = 407.44^\circ$) and $\bar{\lambda}_z = 1.03$ for the human AAA. These are significantly different from the results of the single opening angle experiment.

The main purpose of deriving residual stress levels is to see how they affect the *in vivo* state, i.e. the transmural stresses due to internal pressure and axial tension. The literature shows that residual stresses can either homogenize and decrease them [23], increase them [24] or simply re-distribute the stresses among the layers in a rational way by transferring a larger portion of the stress to the layer designated for this purpose [2]. The specific path taken depends on the material and microstructural properties, on the material model and, what is more important, on the superposition between strains due to residual stress and strains due to *in vivo* forces in a cardiac cycle. Thus, even a small difference in the kinematics of residual deformations may affect the transmural distribution greatly. In other words, when computing residual stresses for specimens exhibiting a non-trivial opening, our optimization strategy can provide a residual kinematical state (based on average residual stresses) that differs significantly from that obtained from the classical opening angle, and therefore will result in *in vivo* stresses that better represent the state of that arterial segment.

Finally, another useful way to interpret these results is to turn to a regional description of the tissues. In some pathologically affected tissues, for example in aneurysms, mechanical and microstructural properties vary along the circumference of the aorta. These variations can be matched with the asymmetric residual openings revealed by our method and used in a comprehensive finite-element analysis for advanced physiological models.

4. Conclusion and limitations

This study proposes, demonstrates and discusses an effective way to approximate residual stresses in circumferential rings that do not open in a trivial and symmetric way; we call it the

'multi-sector approximation method'. The asymmetric shape of the cut configuration is viewed as being composed of several sectors, each with their individual residual stress states. Two examples of such openings are harvested in the laboratory and presented here (pig AA and human AAA), and their residual stresses are derived using both the proposed multi-sector approach and the classical opening angle method.

For both samples, the pig AA and human AAA, the multi-sector approximation method predicts higher residual stresses than the classical opening angle method. Moreover, for the human AAA, it eliminates the uncertainty related to the validity of the sample. In practice, because each sector now has its own residual stress state, the problem can be treated finely using finite-element analysis. Alternatively, for analytical problems and statistical studies, either the averaged response or the peak residual stresses can be used as metrics of overall residual stress levels.

Some limitations apply. In the current approach, the mechanical effect of one sector onto the adjacent sectors is not fully taken into account in either the opened or closed configurations. Basically, the suggested approach treats the opened ring as a number of separate sectors deforming into a number of separate sectors with the same curvature and certain arc-lengths (so that equation (2.4) holds). As a result, there is a stress jump between the sectors, especially when the adjacent sectors undergo different kinds of plane-strain bending (in terms of the bending moment direction), i.e. bending versus unbending.

One way to respect the continuity condition between sectors could be to increase the number of sectors until the jump in stresses becomes negligible. This approach is proposed, for instance, by Matsumoto *et al.* [25], who considered asymmetric residual openings of atherosclerotic thoracic aorta in rabbits, but only in the context of residual strains, not stresses. Their opened rings were split into 32 segments and then the residual strains were derived from the deformations of individual segments. However, this idea cannot be adopted for our approach as these segments stop behaving as sectors owing to an arclength dimension being comparable to the segment's height and thickness.

Another way is to notice that sectors in the opened configuration often exhibit large regions where the curvature is approximately constant and transition regions where the curvature changes rapidly; see figure 2. We could thus optimize our approach by keeping a few large sectors exhibiting constant curvature while splitting transition regions into a large number of segments to approximate continuity, and then computing a weighted average to estimate the residual stress. This approach would solve the continuity issue, but it would be less practical to implement than the simplified solution proposed here, because of its complexity.

The transition regions where the curvature changes abruptly have a more complicated stress state than can be captured by a classical plane-strain bending universal solution that depends on the radial coordinate only. Given that there is geometrical congruence when the ring is closed or residually stressed (and that we cannot predict where the discontinuity in curvature might appear in the opened configuration), we assume that the equilibrium at the edges (or continuity) is achieved by redistribution and concentration of the residual stress originating from microstructural heterogeneity [25]. For example, the mathematical discontinuity

may co-localize with areas that have undergone extensive remodelling with dramatic loss or gain of constituents as is the case for calcification or elastin fragmentation. Our method extracts the residual bending effects from the regions of constant curvature and ignores the vicinities of transition zones instead of speculating on the residual stress state there. This stress state is worthy of further examination, for example by means of experiments which couple microscopy and local strain measurements [26], but this is beyond the scope of this paper.

It is clear from the experiments that the deformed or closed configuration is not exactly circular. Accounting for a non-circular deformed configuration would require digital image splitting of the closed configuration into individual sectors, but this would complicate the analytical solution of the problem and the experiment itself even further.

Also, the way rings open depends on where they are cut. But owing to variation of the circumferential residual deformations along the central line of the aorta, this effect is hard to study experimentally. Moreover, when the opened rings are cut again, they deform even further. This proves that they are still under some level of residual stress, while in our model the cut configuration is split into separate stress-free sectors and, thus, the coupling between them is ignored. Using our approach for newly cut sub-sectors would make sense physically, but would introduce the uncertainty on where to make a cut.

It is well known that if you cut an axial strip from the aorta, it might experience even more notable residual bending deformations than those of a circumferential ring. Our multi-sector approach can be adopted for the determination of residual stresses from these experiments using a block configuration as the deformed one.

Next, our numerical results do not account for the layered structure of blood vessels, but the method can be easily extended to this case.

Also, the residual stresses obtained from our numerical analysis do not account for the material's actual mechanical and microstructural properties, including anisotropy. This choice was made for the sake of simplicity, but the procedure is valid for virtually any strain energy density and more

advanced constitutive models can be used, including properties that vary along the circumference.

Finally, we assumed that the residual deformations originated from a stress-free configuration. If information on the residual deformations is not available, then the strain energy density function can be taken to be a function of not only the deformation gradient \mathbf{F} , but also the residual stress tensor $\boldsymbol{\tau}$, which makes the reference configuration stressed [27,28]. Alternatively, the residual stress can be assumed to arise from differential growth [29] and can then be included into the model using the growth tensor and the multiplicative decomposition rule [30]. Both approaches can be combined as well [31].

The main message of this work is that residual stresses are vital in understanding the development, normal functioning and pathology of biological tissues. Therefore, it is important to have a convenient tool at hand to account for the wide range of sample geometries found in practice, and for the range of tissues that do not deform in a trivial manner when residual stresses are released. This work proposes such a tool as a natural extension of the classical opening angle method. It is capable of dealing with a good number of samples that would have been otherwise eliminated from the analysis.

Ethics. The specimens were collected following a protocol approved by the Conjoint Health Research Ethics Board (CHREB) and the Animal Care Committee (UCARE) at the University of Calgary.

Data accessibility. There are no data associated with this manuscript.

Authors' contributions. All authors contributed equally to the work.

Competing interests. No competing interests.

Funding. We acknowledge funding from the Heart and Stroke Foundation of Canada Grant in Aid G-17-0019141.

Acknowledgements. This publication was made possible by a James M Flaherty Research Scholarship from the Ireland Canada University Foundation, with the assistance of the Government of Canada/avec l'appui du gouvernement du Canada. The authors gratefully acknowledge Dr Randy Moore, Peter Loughheed Centre and Cheryl Hall, Dr. J. Tyberg's laboratory, Department of Cardiac Sciences, University of Calgary, Calgary, Alberta, for surgical specimen collection. Finally, we thank the anonymous referees for invaluable help in improving a draft version of the paper.

Reference

1. Destrade M, Liu Y, Murphy JG, Kassab GS. 2012 Uniform transmural strain in pre-stressed arteries occurs at physiological pressure. *J. Theor. Biol.* **303**, 93–97. (doi:10.1016/j.jtbi.2012.03.010)
2. Sigaeva T, Sommer G, Holzapfel GA, Di Martino ES. 2019 Anisotropic residual stresses. *J. R. Soc. Interface* **16**, 20190029. (doi:10.1098/rsif.2019.0029)
3. Vaishnav RN, Vossoughi J. 1983 Estimation of residual strains in aortic segments. In *Biomedical engineering II* (ed. CW Hall), pp. 330–333. Elmsford, NY: Pergamon Press.
4. Fung YC. 1984 *Biomechanics: circulation*. Berlin, Germany: Springer Science & Business Media.
5. Chuong CJ, Fung YC. 1986 Residual stress in arteries. In *Frontiers in biomechanics* (eds GW Schmid-Schönbein, SLY Woo, BW Zweifach), pp. 117–129. New York, NY: Springer.
6. Nelson D. 2014 Experimental methods for determining residual stresses and strains in various biological structures. *Exp. Mech.* **54**, 695–708. (doi:10.1007/s11340-013-9806-6)
7. Cardamone L, Valentin A, Eberth JF, Humphrey JD. 2009 Origin of axial prestretch and residual stress in arteries. *Biomech. Model. Mechanobiol.* **8**, 431–446. (doi:10.1007/s10237-008-0146-x)
8. Holzapfel GA, Ogden RW. 2010 Modelling the layer-specific three-dimensional residual stresses in arteries, with an application to the human aorta. *J. R. Soc. Interface* **7**, 787–799. (doi:10.1098/rsif.2009.0357)
9. Holzapfel GA, Sommer G, Auer M, Regitnig P, Ogden RW. 2007 Layer-specific 3D residual deformations of human aortas with non-atherosclerotic intimal thickening. *Ann. Biomed. Eng.* **35**, 530–545. (doi:10.1007/s10439-006-9252-z)
10. Pena JA, Martinez MA, Pena E. 2015 Layer-specific residual deformations and uniaxial and biaxial mechanical properties of thoracic porcine aorta. *J. Mech. Behav. Biomed. Mater.* **50**, 55–69. (doi:10.1016/j.jmbm.2015.05.024)
11. Rivlin RS, Barenblatt GI, Joseph DD. 1997 *Collected papers of RS Rivlin*. Berlin, Germany: Springer Science & Business Media.
12. Fung YC. 1991 What are the residual stresses doing in our blood vessels? *Ann. Biomed. Eng.* **19**, 237–249. (doi:10.1007/BF02584301)
13. Liu SQ, Fung YC. 1989 Relationship between hypertension, hypertrophy, and opening angle of zero-stress state of arteries following aortic

- constriction. *J. Biomech. Eng.* **111**, 325–335. (doi:10.1115/1.3168386)
14. Sokolis DP, Savva GD, Papadodima SA, Kourkoulis SK. 2017 Regional distribution of circumferential residual strains in the human aorta according to age and gender. *J. Mech. Behav. Biomed. Mater.* **67**, 87–100. (doi:10.1016/j.jmbbm.2016.12.003)
 15. Iliopoulos DC, Deveja RP, Kritharis EP, Perrea D, Sionis GD, Toutouzas K, Stefanadis C, Sokolis DP. 2009 Regional and directional variations in the mechanical properties of ascending thoracic aortic aneurysms. *Med. Eng. Phys.* **31**, 1–9. (doi:10.1016/j.medengphy.2008.03.002)
 16. Liu SQ, Fung YC. 1988 Zero-stress states of arteries. *J. Biomech. Eng.* **110**, 82–84. (doi:10.1115/1.3108410)
 17. Fung YC, Liu SQ. 1989 Change of residual strains in arteries due to hypertrophy caused by aortic constriction. *Circ. Res.* **65**, 1340–1349. (doi:10.1161/01.RES.65.5.1340)
 18. Sokolis DP. 2015 Effects of aneurysm on the directional, regional, and layer distribution of residual strains in ascending thoracic aorta. *J. Mech. Behav. Biomed. Mater.* **46**, 229–243. (doi:10.1016/j.jmbbm.2015.01.024)
 19. Okamoto RJ, Wagenseil JE, DeLong WR, Peterson SJ, Kouchoukos NT, Sundt TM. 2002 Mechanical properties of dilated human ascending aorta. *Ann. Biomed. Eng.* **30**, 624–635. (doi:10.1114/1.1484220)
 20. Sigaeva T, Mangan R, Vergori L, Destrade M, Sudak L. 2018 Wrinkles and creases in the bending, unbending and eversion of soft sectors. *Proc. R. Soc. A* **474**, 20170827. (doi:10.1098/rspa.2017.0827)
 21. Sigaeva T. 2018 Note on the generality of one plane strain bending universal solution. *Mech. Res. Commun.* **94**, 120–124. (doi:10.1016/j.mechrescom.2018.10.005)
 22. Young D. 2016 Hough transform for circles. MATLAB Central File Exchange (retrieved 4 March 2016). See <https://www.mathworks.com/matlabcentral/fileexchange/26978-hough-transform-for-circles>.
 23. Ciarletta P, Destrade M, Gower AL. 2016 On residual stresses and homeostasis: an elastic theory of functional adaptation in living matter. *Sci. Rep.* **6**, 24390. (doi:10.1038/srep24390)
 24. Labrosse MR, Gerson ER, Veinot JP, Beller CJ. 2013 Mechanical characterization of human aortas from pressurization testing and a paradigm shift for circumferential residual stress. *J. Mech. Behav. Biomed. Mater.* **17**, 44–55. (doi:10.1016/j.jmbbm.2012.08.004)
 25. Matsumoto T, Hayashi K, Ide K. 1995 Residual strain and local strain distributions in the rabbit atherosclerotic aorta. *J. Biomech.* **28**, 1207–1217. (doi:10.1016/0021-9290(94)00179-8)
 26. Matsumoto T, Goto T, Furukawa T, Sato M. 2004 Residual stress and strain in the lamellar unit of the porcine aorta: experiment and analysis. *J. Biomech.* **37**, 807–815. (doi:10.1016/j.jbiomech.2003.08.014)
 27. Shams M, Destrade M, Ogden RW. 2011 Initial stresses in elastic solids: constitutive laws and acoustoelasticity. *Wave Motion* **48**, 552–567. (doi:10.1016/j.wavemoti.2011.04.004)
 28. Merodio J, Ogden RW. 2014 Extension, inflation and torsion of a residually stressed circular cylindrical tube. *Continuum Mech. Thermodyn.* **28**, 157–174. (doi:10.1007/s00161-015-0411-z)
 29. Vandiver R, Goriely A. 2009 Differential growth and residual stress in cylindrical elastic structures. *Phil. Trans. R. Soc. A* **367**, 3607–3630. (doi:10.1098/rsta.2009.0114)
 30. Rodriguez EK, Hoger A, McCulloch AD. 1994 Stress-dependent finite growth in soft elastic tissues. *J. Biomech.* **27**, 455–467. (doi:10.1016/0021-9290(94)90021-3)
 31. Du Y, Lü C, Chen W, Destrade M. 2018 Modified multiplicative decomposition model for tissue growth: beyond the initial stress-free state. *J. Mech. Phys. Solids* **118**, 133–151. (doi:10.1016/j.jmps.2018.05.014)